

Lattice-mismatch-induced granularity in CoPt-NbN and NbN-CoPt superconductor-ferromagnet heterostructures: Effect of strain.

R. K. Rakshit, S. K. Bose, R. Sharma, N. K. Pandey, and R. C. Budhani*

Condensed Matter - Low Dimensional Systems Laboratory, Department of Physics,

Indian Institute of Technology Kanpur, Kanpur - 208016, India

Abstract

The effect of strain due to lattice mismatch and of ferromagnetic (FM) exchange field on superconductivity (SC) in NbN-CoPt bilayers is investigated. Two different bilayer systems with reversed deposition sequence are grown on MgO (001) single crystals. While robust superconductivity with high critical temperature ($T_c \approx 15.3$ K) and narrow transition width ($\Delta T_c \approx 0.4$ K) is seen in two types of CoPt-NbN/MgO heterostructures where the magnetic anisotropy of CoPt is in-plane in one case and out-of-plane in the other, the NbN-CoPt/MgO system shows markedly suppressed SC response. The reduced SC order parameter of this system, which manifests itself in T_c , temperature dependence of critical current density J_c (T), and angular (ϕ) variation of flux-flow resistivity ρ_f is shown to be a signature of the structure of NbN film and not a result of the exchange field of CoPt. The ρ_f (H,T, ϕ) data further suggest that the domain walls in the CoPt film are of the Néel type and hence do not cause any flux in the superconducting layer. A small, but distinct increase in the low-field critical current of the CoPt-NbN couple is seen when the magnetic layer has perpendicular anisotropy.

I. INTRODUCTION

Hybrid superconductor-ferromagnet (SC-FM) structures have generated a considerable amount of interest in recent years as these provide model systems to understand the antagonism between superconductivity and ferromagnetism^{1,2,3,4,5,6,7,8,9,10,11,12,13,14,15,16,17,18,19}.

A rich variety of phenomena such as π -phase shift^{1,2}, triplet pairing^{2,3}, field enhanced superconductivity^{4,5}, domain wall superconductivity⁶ and enhanced flux pinning^{7,8,9,10,11} etc.

have been reported in SC-FM structures. An important issue that needs to be considered while addressing the physics of SC-FM-SC and FM-SC-FM heterostructures is the difference in the crystallographic structure and the degree of strain in the top and bottom SC or FM layers, and interdiffusion at interfaces which could impart different physical properties to the top and bottom layers. The other issue related to the physics of SC-FM junctions is the choice of materials. Thus far most of the studies in this area have been carried out on heterostructures of elemental superconductors such as Pb and Nb made in conjunction with 3d transition metal ferromagnets^{4,6,11,12,13,14}. It is expected that the competition between the SC and FM orders will have a different flavor if hard superconductors characterized by a short coherence length and large magnetic penetration depth are used. The nature of

magnetic layers is also not less important as field enhanced superconductivity and vortex pinning depend greatly on the domain structure and dynamics of domain wall motion in the magnetic layer¹⁰.

Here we report investigations of domain wall superconductivity, flux pinning and granularity issues in a strongly type-II superconductor placed in close proximity of a magnetic thin film. The system investigated consists of a bilayer of A1 phase (fcc) or L1₀ phase (fct) CoPt ferromagnet and NbN (rocksalt) superconductor grown on MgO (001). NbN and CoPt were chosen as constituents of the SC-FM bilayer since their respective superconducting and magnetic properties can be modified in a controlled way by altering the deposition conditions^{21,22,23}. Two different bilayer systems with reversed deposition sequence have been investigated to address superconductivity and magnetism vis-a-vis crystallographic structure and exchange field-induced proximity effects. We note that while the lattice mismatch has a minor effect on superconductivity of the bottom NbN layer in CoPt-NbN/MgO system, in the NbN-CoPt/MgO bilayer it makes the NbN film to adopt a strain-induced granular structure, which has interesting repercussions on its superconducting response. We see a small but distinct enhancement in the low-field critical current density (J_c) of the CoPt-NbN/MgO

bilayer when the CoPt has perpendicular magnetic anisotropy.

II. EXPERIMENTAL

The CoPt-NbN/MgO and NbN-CoPt/MgO bilayers with 50 nm thick CoPt and NbN layers in each case were deposited on (001) MgO in the temperature range of 600 to 700 °C by pulsed laser ablation of Nb and CoPt targets in 99.9999 % pure nitrogen environment. A distinctly different magnetic state of the CoPt is realized when the deposition temperature is elevated from 600 to 700 °C. At the lower temperature, the CoPt is in the disordered fcc phase (A1) with in-plane magnetization whereas, at 700 °C it acquires the ordered L1₀ structure with out-of-plane magnetic anisotropy²⁰. Further details of CoPt and NbN growth have been reported earlier^{21,22,23}. The crystal structure of bilayer films was investigated by X-ray diffraction (XRD) measurements performed on a θ - ω diffractometer with CuK _{α 1, α 2} radiation. The surface topography of the bilayers was analyzed using high resolution scanning electron microscopy (SEM), which showed a smooth morphology for the CoPt-NbN/MgO system but a granular structure with typical feature size of 75 to 100 nm in NbN-CoPt/MgO bilayer. Measurements of AC susceptibility were performed with a Hall-probe-based ac susceptometer, which is described in detail elsewhere²⁴. For measurements of

magnetoresistance and critical current density (J_c), samples were processed using standard photolithography and Ar^+ ion milling to produce 500 μm long and 160 μm wide bridges. After removing the photoresist, silver pads for electrical contact were deposited in a four-probe configuration by thermal evaporation. The resistance of the samples in the flux flow regime was also measured as a function of the angle ϕ between the applied magnetic field and film normal. While the angle in these measurements was changed in a step of 2 degree, the field always remained orthogonal to the current direction. A commercial magnetometer (Quantum Design MPMS-XL5) was used for measurements of in-plane and out-of-plane isothermal magnetization above and below the superconducting transition temperature of the bilayers.

III. RESULTS AND DISCUSSION

A. Bilayers with in-plane magnetic anisotropy

In Fig. 1(a) we have plotted the temperature dependence of resistance of the two bilayers, deposited at 600 $^{\circ}\text{C}$ along with data for a pure NbN film for comparison. The latter shows a sharp transition ($\Delta T_c \approx 0.4$ K) with the onset of superconductivity at 15.5 K. The CoPt-NbN/MgO bilayer also displays a sharp transition of width ≈ 0.4 K with T_c onset at 15.3

K. The other bilayer (NbN-CoPt/MgO), however, has a substantially reduced T_c (≈ 13.7 K) and a sizeable broadening of the transition (≈ 1.4 K).

Fig. 1(b) shows the real and imaginary components of the fundamental susceptibility of the same samples. The frequency, and amplitude of the ac field applied perpendicular to the plane of the film, in these experiments are 121 Hz and 1 Oe, respectively. The real part $\chi' (T)$ of the complex susceptibility $\chi (T) = \chi' (T) + i\chi'' (T)$ reflects the strength of the induced shielding currents, while the imaginary part $\chi'' (T)$ is connected to energy dissipation in the material. The drop of $\chi' (T)$ whose onset corresponds to the temperature where the resistance (R) goes to zero is reasonably sharp for both pure NbN film as well as for the CoPt-NbN/MgO bilayer, indicating a homogeneous superconductor. However, for the bilayer where the NbN is deposited on top of CoPt, both χ' and χ'' show significant broadening. For inhomogeneous superconductor with distinctly different intergrain and intragrain critical currents, the χ'' peak generally splits into two components each corresponding to peak dissipation in superconducting grains and in intergranular material²⁵. The fact that we do not see two distinct peaks in the χ'' data for NbN-CoPt/MgO system suggests insignificant suppression of the order parameter in the intergrain material of the NbN layer. However, the

overall suppression of T_c seen here compared to the T_c of the bilayer where NbN is deposited first, seems to indicate a perturbation of the electronic structure by stress or chemical doping which lowers the critical temperature. In order to address these issues, we have undertaken X-ray diffraction studies of the bilayer films.

Fig. 2 (Panel ‘a’ and ‘b’ respectively) shows the diffraction profiles of NbN-CoPt/MgO and CoPt-NbN/MgO along with the profiles of single layer CoPt (panel ‘c’), NbN (panel ‘d’) and bare MgO substrate (panel ‘e’). The single layer CoPt film shows only one peak at $2\theta = 48.13^\circ$ which corresponds to the (200) reflection of the disordered A1 (fcc) phase. Single layer NbN also shows the characteristic (200) and (400) reflections of the fcc phase indicating a highly textured growth along [001] direction of MgO. While all these characteristic reflections of the [001] growth are seen in CoPt-NbN/MgO bilayer (panel ‘b’) as well, the NbN peaks are not discernible in the reverse bilayer geometry (panel ‘a’), where NbN was grown on CoPt, suggesting a granular structure of the nitride. These results reveal that film growth dynamics is greatly controlled by the amount of interfacial strain induced by the cubic (100) MgO whose lattice parameter ‘a’ is 4.21 Å. NbN is also cubic with $a = 4.39$ Å. The magnetic alloy CoPt, when grown on (100) MgO at ≤ 600 °C has a disordered fcc structure with a

lattice parameter of 3.772 \AA ²⁶. The lattice mismatch for epitaxial growth of ‘A’ on ‘B’ can be characterized in terms of the strain parameter ϵ defined as $\epsilon = \frac{d_A - d_B}{d_A} \times 100$ where, d_A and d_B are the lattice parameters of ‘A’ and ‘B’ respectively. This gives ϵ of $\approx 4.1 \%$, $\approx -11.6 \%$, $\approx -16.4 \%$ and $\approx 14.1 \%$ for NbN-MgO, CoPt-MgO, CoPt-NbN and NbN-CoPt systems respectively. In Fig. 3 we sketch the stacking of the unstrained unit cells in NbN, CoPt and MgO starting with MgO at the bottom. Dotted lines in the figure represents ideal coherent epitaxy in conformity with the substrate. The origin of in-plane tensile strain on CoPt and compressive strain on NbN under coherent epitaxy can be visualized from this figure.

It is interesting to note that in spite of a large strain parameter ($\epsilon \approx -16.4 \%$), CoPt prefers to grow epitaxially with a slight change ($\approx 0.2 \%$) in lattice parameter from bulk when deposited on NbN [Fig. 2(b)]. The peak shift [$\Delta\theta \approx 0.1^\circ$] of the (200) reflection of CoPt grown on NbN/MgO can be attributed to an improper growth due to mismatch. On the other hand, the large compressive strain ($\sim 14.1 \%$) experienced by NbN, when deposited on CoPt as compared to only $\approx 4.1 \%$ when grown directly on MgO, forces a highly disordered growth of NbN. We believe that the rough surface texture of CoPt films on MgO as seen in our scanning electron microscopy studies and originating presumably

from strain ($\epsilon \approx -11.6\%$) makes the subsequent growth of NbN disordered.

In Fig. 4 (a & b) we have shown isothermal magnetization at 20 K as a function of in-plane magnetic field for the bilayers, along with the data for resistance. We note that at 20 K the coercive field (H_c) of the CoPt-NbN/MgO system is ≈ 250 Oe, which is lower than the H_c of the NbN-CoPt/MgO bilayer (≈ 500 Oe) as seen in the M-H loop of Fig. 4(b).

This can be understood in the following way. During the growth of the 50 nm thick NbN using the deposition conditions mentioned before, the bottom CoPt layer gets annealed for roughly about 7 - 8 minutes, which leads to a better ordering of the structure as evidenced by the enhanced intensity of (200) reflection of the A1 phase (see Fig.2 patterns 'a' and 'b').

This observation is consistent with previous studies on CoPt system which reveal that the 600 °C deposited films consist of only the fcc phase and their coercive field increases with the duration of postdeposition annealing²².

The isothermal resistance of the samples in the normal state (20 K) when a dc field aligned parallel to the plane of the film and directed perpendicular to current was scanned between + 3.5 kOe and - 3.5 kOe is also shown in Fig. 4. Arrows in the figure mark the increasing and decreasing branches of the field. For the CoPt-NbN/MgO bilayer (Fig. 4(a)) upon

reducing the field from 3.5 kOe, where the magnetization reaches saturation and the sample is presumably in a single domain state, the resistance decreases smoothly with field, i.e., dR/dH is positive. This behavior gives way to a sudden jump in resistance when the sample reaches a truly demagnetized state at $H = H_c$. We attribute this effect to enhanced domain wall scattering of charge carriers which presumably also leads to the observed superlinear dependence of R on the increasing $|H|$ branch till the saturation field H_s is reached. For $H > H_s$, the resistance rises in a sublinear fashion. In the other bilayer, where CoPt is at the bottom, the hysteresis in the resistivity is much more pronounced.

The M-H curves of the bilayers change dramatically on entering the superconducting state as seen in Fig. 5. These data were taken at 5 K with in-plane field. For the CoPt-NbN/MgO bilayer, the M-H curve is dominated by the diamagnetic response of the superconducting NbN layer, showing a hysteresis loop typical of a type-II superconductor. However, for the NbN-CoPt/MgO bilayer, the ferromagnetic component of magnetization is distinctly seen. The sudden jump in magnetization at ± 500 Oe coincides exactly with the coercive field (H_c) seen in the M-H loop taken at 20 K (Fig. 4(b)). Since the moment of CoPt is not expected to change below 20 K because of its large Curie temperature (≈ 710 K)²⁷, the true

diamagnetic response of the superconductor can be extracted by subtracting the 20 K data from the 5 K data. The continuous M-H curves in Fig. 5 (a & b) are the true diamagnetic response. We can use the Bean critical state model²⁵ to extract the screening critical current density J_c from these M-H data. At field $H \approx 550$ Oe which is larger than the coercive field of both type of bilayers, the J_c of CoPt-NbN/MgO system is larger by a factor of $\simeq 3.5$ compared to the J_c of the NbN-CoPt/MgO heterostructure. The large suppression of J_c in the latter structure suggests a granular character of its NbN layer. It is worth pointing out that the actual flux density in these films of thickness (≈ 50 nm) smaller than the London penetration depth ($\approx 200 - 250$ nm) will be lower due to the dipolar field of the CoPt layer which induces reverse flux. However, the presence of the ferromagnetic layer will not affect the relative magnitude of J_c in the two cases as long as the field is greater than the coercive field.

Now we discuss how the superconductivity in a granular and a homogeneous film is affected when it is placed in proximity of a ferromagnet with in-plane magnetization through measurement of transport critical current density and its temperature and angular dependence. Fig. 6(a) presents the J_c measured with a voltage criterion of $10 \mu\text{V}/\text{cm}$ as a function

of reduced temperature (T/T_c) for both the bilayers and a single layer NbN film. Here T_c denotes the temperature corresponding to the zero resistance state of the samples. For the bilayer sample CoPt-NbN/MgO, the J_c at $T/T_c \geq 0.9$ is same ($\approx 6.0 \times 10^5$ A/cm²) as that of a single layer NbN film and below $T/T_c = 0.9$, it exceeds the limit of our measurement which is set by the maximum output of our current source (~ 100 mA). For the other bilayer film (NbN-CoPt/MgO) however, the J_c is highly suppressed. For example, at $T/T_c = 0.8$ it is only $\approx 1.5 \times 10^5$ A/cm². Fig. 6 also shows the J_c vs. T/T_c plots of the two bilayers when a 300 Oe field is applied perpendicular to the plane of the film. We note that the field-induced suppression of J_c is marginally higher in the case of NbN-CoPt/MgO heterostructure. The temperature dependence of J_c is generally expressed by a phenomenal expression of the type,

$$J_c = J_0(1 - T/T_c)^\beta, \quad (1)$$

where J_0 and β are used as fitting parameters. In the Ginzburg-Landau (GL) mean-field description of J_c , the prefactor J_0 is a measure of the depairing current and the exponent β is $3/2$ ²⁸. For a highly granular system where superconducting grains are separated by insulating material, the Ambegaokar-Baratoff model can be used to describe the J_c (T) data²⁸. Here J_0 is related to superconducting gap parameter and the exponent $\beta \approx 1$ at low

temperatures. The data shown in Fig. 6 have been fitted to Eq. 1. The J_0 and β for the NbN/MgO, CoPt-NbN/MgO and NbN-CoPt/MgO in zero field are ($\approx 7.81 \times 10^6$ A/cm², 0.93), ($\approx 1.65 \times 10^7$ A/cm², 1.19) and ($\approx 1.64 \times 10^6$ A/cm², 1.40) respectively. For the first two samples, since the fitting has been done over a very limited range of T/T_c , too much significance can not be given to J_0 and β . However, for NbN-CoPt/MgO excellent fitting is seen for T/T_c ranging from 0.5 to ≈ 1 . It is interesting to note that while the NbN in this sample has a substantially reduced J_c , the β remains close to the GL value. The large value of β here suggests a robust coupling between NbN grains²⁸.

In order to examine how the state of magnetization of the CoPt film affects superconductivity in NbN, we have measured the temperature dependence of J_c with in-plane field [Fig. 6(b)] corresponding to points A and B of the hysteresis loop as shown in the inset of Fig. 6(b). Since at point A of the loop the sample is fully saturated, it should behave like a single domain magnetic entity. Point B of the loop corresponds to a fully demagnetized state where the sample consists of randomly oriented domains. The direction of magnetization from one domain to the next can change either by out-of-plane rotation of spins, which constitutes a Bloch wall or by in-plane rotation as in the case of a Néel wall²⁹. Obviously,

a Bloch wall will lead to magnetic flux into the NbN layer where as for a Néel wall the flux remains confined in the ferromagnetic film. A Bloch wall is therefore expected to reduce the J_c of the film. The J_c of the NbN-CoPt/MgO and CoPt-NbN/MgO films measured at positions A and B of the hysteresis loop is shown in Fig. 6(b). No discernible difference in the critical current in the two cases is seen suggesting that in these 50 nm CoPt films the domain walls are of Néel type.

In order to address further the likely perturbation of superconductivity in NbN by magnetic domain structure of CoPt layer, we show in Fig. 7 the angular dependence of flux flow resistivity at three points of the hysteresis loop measured at a temperature where resistance drops by ≈ 95 % of its normal state value in zero-field. The orientation of current \vec{I} , magnetization \vec{M} and magnetic field \vec{H} vectors are shown in the inset of the figure. The angle ϕ is between \vec{H} and film normal \hat{n} . At saturation points A and D of the loop the \vec{M} vector is always perpendicular to \vec{J} , either along $+\hat{y}$ or $-\hat{y}$. The flux flow resistivity of both bilayers at $H = \pm 1500$ Oe (points A and D of hysteresis) is characterized by two sharp cusps at $\phi = \pm 90^\circ$ and maximum dissipation at $\phi = 0^\circ$, i.e., when the field is normal to the film surface. If we attribute the flux flow resistivity only to the normal component of the field

($H\cos\phi$), then ρ_f must go linearly in $H\cos\phi$ following the relation for flux flow resistance

$\rho_f/\rho_N \approx H/H_{c2}$, where ρ_N is the normal state resistance and H_{c2} the upper critical field³⁰.

In the right inset of Fig. 7 we show variation of ρ_f vs. $H\cos\phi$ for CoPt-NbN/MgO and NbN-CoPt/MgO bilayers. In the former case, where superconductivity is robust in NbN, the flux-flow resistance shows a linear dependence on $H\cos\phi$. For the sample where NbN is on the top, however, the scaling of ρ_f with $H\cos\phi$ is poor, indicating that this film can not be treated as an infinite superconducting plane. In Fig. 7 we have also plotted the angular dependence of R_f at points B and C of the hysteresis loop. The large dissipation seen at the coercive field in NbN-CoPt/MgO over a range of angles around $\phi = 0$ again points towards the granular nature of the NbN.

B. Bilayers with out-of-plane magnetic anisotropy

Equiatomic CoPt films deposited at 700 °C on MgO stabilize into the $L1_0$ (tetragonal) ordered structure with a strong out-of-plane anisotropy energy ($\approx 5 \times 10^6$ J/m³)³¹. It is expected that the magnetic domain structure of such films can lead to strong pinning of vortices in a field range below the coercive field of the ferromagnet^{8,10}. We have compared the relative influence of $L1_0$ and A1 disordered CoPt layers on flux pinning in NbN in a

controlled experiment in which a 50 nm NbN film was first grown at 700 °C on three MgO substrates mounted side-by-side in the deposition chamber. On one of such films a 50 nm CoPt was deposited at 700 °C followed by annealing in high vacuum for 30 minutes while on the other the CoPt layer of the same thickness was deposited at 600 °C, but after annealing the NbN at 700 °C for a time equal to the postannealing time used for L1₀ CoPt growth (\approx 30 minutes). The third film was also annealed for 40 minutes at 700 °C under the identical conditions to ensure the same metallurgical state of the NbN in all three samples. In Fig. 8 we show superconducting transition of these films measured resistively. While the T_c onset of the bare NbN is \approx 15.5 K, a suppression of the critical temperature by \approx 0.2 K is seen on deposition of the two-types of CoPt. This lowering of T_c perhaps derives contribution from exchange-field-induced pair-breaking in NbN. From the X-ray diffraction pattern shown in inset ‘a’ of Fig. 8, it becomes clear that CoPt films grown at 600 and 700 °C on NbN are in the A1 (fcc) and L1₀ (tetragonal) polytypes with their (001) direction normal to the plane of the film. Inset ‘b’ of Fig. 8 shows magnetic hysteresis loop of these two bilayers measured at 20 K with the external field directed perpendicular to the film plane. The square loop of the film deposited at 700 °C clearly indicates out-of-plane magnetic anisotropy axis with

coercivity ≈ 5 kOe. Having established the distinct magnetic and crystallographic structure of the CoPt, we address the issue of flux pinning in these bilayers. In Fig. 9 we compare the critical current density of the NbN films with A1 and L1₀ CoPt capping layer at three temperatures very close to T_c ($T/T_c \geq 0.92$) and in a field range $H \ll H_c$ of the L1₀ film. The magnetic field was directed perpendicular to the plane of the film. It is very clear that the L1₀ CoPt-NbN couple has a small but distinctly larger J_c as compared to that of the A1 CoPt-NbN in a field range $H < 1$ kOe ($\ll H_c$). To emphasize this increase, in the inset of Fig. 9 we plot $\Delta J_c = [J_c (L1_0) - J_c(A1)]$. This enhancement of critical current can be explained qualitatively in the framework of the model of Bulaevskii, Chudnovsky and Maley (BCM)¹⁷ which shows that a flux line in superconducting film capped with a magnetic layer of perpendicular anisotropy experiences a spatially modulated pinning barrier of the type $U_{mp}(x) \sim \Phi_0 M(x) d_s$, where Φ_0 is the flux quantum, $M(x)$, the magnetization of the FM domain and d_s the superconducting film thickness. This behavior is relevant when the vortex motion is perpendicular to domain wall, and the width of the domain l is large compared to d_s and magnetic penetration depth $\lambda_L \ll l$. Both these conditions are satisfied by the CoPt film. The J_c expected from such domain wall pinning is $\sim c M_0/l$; with $M_0 \approx 450$

emu/cc for our L1₀ CoPt film, and $l \approx 1000$ nm, we get $J_c \sim 4.5 \times 10^7$ A/cm² for vortex motion perpendicular to domain walls. In real samples, however, the domains have arbitrary geometry in which vortices gliding along domain walls will experience no pinning force and thus a much smaller increase in J_c would result. For the A1 CoPt film, the perpendicular component of magnetization at $H = 1$ kOe, where a detectable enhancement in J_c is seen, is very small and we do not expect any magnetic pinning in this case.

In summary, we have studied the crystallographic structure, magnetic ordering and superconducting properties of ferromagnet-superconductor bilayers made of CoPt and NbN grown on single crystal MgO in two different geometries, with either NbN or CoPt in contact with the substrate. In the case of bilayers where CoPt is deposited over NbN, a further distinction has been realized by selecting ordered (L1₀) or disordered (A1) polytypes of CoPt showing in-plane and perpendicular magnetic anisotropy respectively. By comparing the SC response of bilayers where the CoPt magnetization is in the plane of the structure with that of a plane NbN film, we conclude that the ferromagnetism of CoPt has no discernible effect on the bulk SC properties of the NbN. This also leads us to believe that the magnetic domain walls in A1 CoPt of both bilayers are of the Néel type. While the ferromagnetism of CoPt

has no deleterious effects, the polycrystalline nature of NbN deposited on CoPt imparts it a granular character which reflects itself in a reduced T_c , in the temperature dependence of J_c , and in the variation of flux-flow resistance as a function of the angle between applied field and film normal. A comparison of critical current density in CoPt-NbN/MgO bilayers show a distinctly higher J_c in samples where the CoPt magnetization is out-of-plane. Since this gain is seen only at fields smaller than the coercivity of the CoPt layer, we attribute it to domain wall pinning of flux lines.

This research has been supported by grants from the Department of Science & Technology under its Nanoscience & Nanotechnology Initiative and by the Board for Research in Nuclear Science. S. K. Bose acknowledges financial support from the Council for Scientific and Industrial Research, Government of India. We also acknowledge Mr. Pooran C. Joshi for his technical assistance.

* Electronic address: rcb@iitk.ac.in

¹ V. V. Ryazanov, V. A. Oboznov, A. Yu. Rusanov, A. V. Veretennikov, A. A. Golubov, and J. Aarts, Phys. Rev. Lett. **86**, 2427 (2001).

² A. I. Buzdin, Rev. Mod. Phys. **77**, 935 (2005).

³ A. F. Volkov, F. S. Bergeret, and K. B. Efetov, Phys. Rev. Lett. **90**, 117006 (2003).

⁴ M. Lange, M. J. Van Bael, Y. Bruynseraede, and V. V. Moshchalkov, Phys. Rev. Lett. **90**,

- 197006 (2003).
- ⁵ J. Y. Gu, C.-Y. You, J. S. Jiang, J. Pearson, Y. B. Bazaliy, and S. D. Bader, Phys. Rev. Lett. **89**, 267001 (2002).
 - ⁶ W. Gillijns, A. Y. Aladyshkin, M. Lange, M. J. Van Bael, and V. V. Moshchalkov, Phys. Rev. Lett. **95**, 227003 (2005).
 - ⁷ A. García-Santiago, F. Sánchez, M. Varela, and J. Tejada, Appl. Phys. Lett. **77**, 2900 (2000).
 - ⁸ D. B. Jan, J. Y. Coulter, M. E. Hawley, L. N. Bulaevskii, M. P. Maley, Q. X. Jia, B. B. Maranville, F. Hellman, and Q. X. Pan, Appl. Phys. Lett. **82**, 778 (2003).
 - ⁹ M. Z. Cieplak, X. M. Cheng, C. L. Chien, and H. Sang, J. Appl. Phys. **97**, 026105 (2005).
 - ¹⁰ M. Lange, M. J. Van Bael, V. V. Moshchalkov, and Y. Bruynseraede, Appl. Phys. Lett. **81**, 322 (2002).
 - ¹¹ M. I. Montero, J. J. Akerman, A. Varilci, and I. K. Schuller, Europhys. Lett. **63**, 118 (2003).
 - ¹² R. J. Kinsey, G. Burnell, and M. G. Blamire, IEEE Trans. Appl. Supercond. **11**, 904 (2001).
 - ¹³ J. I. Martín, M. Vélez, J. Nogués, and I. K. Schuller, Phys. Rev. Lett. **79**, 1929 (1997).
 - ¹⁴ A. Palau, H. Parvaneh, N. A. Stelmashenko, H. Wang, J. L. Macmanus-Driscoll, and M. G. Blamire, Phys. Rev. Lett. **98**, 117003 (2007).
 - ¹⁵ K. Senapati and R. C. Budhani, Phys. Rev. B **70**, 174506 (2004).
 - ¹⁶ M. D. Allsworth, R. A. Chakalov, M. S. Colclough, P. Mikheenko, and C. M. Muirhead, Appl. Phys. Lett. **80**, 4196 (2002).
 - ¹⁷ L. N. Bulkaevskii, E. M. Chudnovsky, and M. P. Maley, Appl. Phys. Lett. **76**, 2594 (2000).
 - ¹⁸ A. Yu. Rusanov, M. Hesselberth, J. Aarts, and A. I. Buzdin, Phys. Rev. Lett. **93**, 057002 (2004).
 - ¹⁹ D. Stamopoulos, and E. Manios, Supercond. Sci. Technol. **18**, 538 (2005).
 - ²⁰ K. Barmak, J. Kim, L. H. Lewis, K. R. Coffey, M. F. Toney, A. J. Kellock, and J. -U. Thiele, J. Appl. Phys. **98**, 033904 (2005).
 - ²¹ R. K. Rakshit, S. K. Bose, R. Sharma, and R. C. Budhani, Appl. Phys. Lett. **89**, 202511 (2006).
 - ²² R. K. Rakshit, S. K. Bose, R. Sharma, R. C. Budhani, T. Vijaykumar, S. J. Neena, and G. U. Kulkarni, J. Appl. Phys. **103**, 023915 (2008).
 - ²³ K. Senapati, N. K. Pandey, R. Nagar, and R. C. Budhani, Phys. Rev. B **74**, 104514 (2006).
 - ²⁴ K. Senapati, S. Chakrabarty, Leena K. Sahoo, and R. C. Budhani, Rev. Sci. Instrum. **75**, 141 (2004).
 - ²⁵ J. H. Classen, in *Magnetic Susceptibility of Superconductor and Other Spin Systems*, edited by

- R. A. Hein, T. L. Francavilla, and D. H. Liebenberg (Plenum, New York, 1991), p.405
- ²⁶ J. M. Pennison, A. Bourret, and A. Ph. Eurin, *Acta Metall.* **19**, 1195 (1971).
- ²⁷ A. Kootte, C. Haas, and R. A. de Groot, *J. Phys.: Condens. Matter* **3**, 1133 (1991).
- ²⁸ J. R. Clem, B. Bumble, S. I. Raider, W. J. Gallagher, and Y. C. Shih, *Phys. Rev. B* **35**, 6637 (1987).
- ²⁹ Robert C. O’Handley, *Modern Magnetic Materials Principles and Applications*, (John Wiley and Sons, Inc., New York 2000), chap. 8, p. 275.
- ³⁰ M. Tinkham *Introduction to Superconductivity* (McGraw-Hill, Inc. Singapore, 1996), p. 166.
- ³¹ R. A. McCurrie and P. Gaunt, *Philos. Mag.* **13**, 567 (1966).

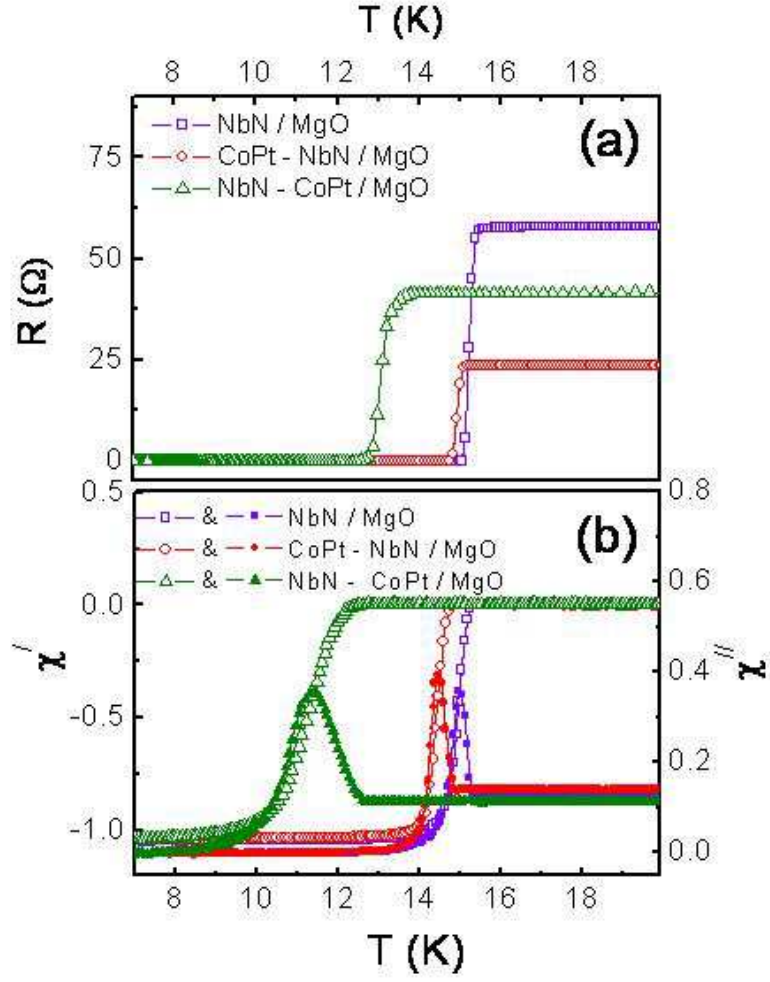


FIG. 1: Panel (a) shows the temperature dependence of resistance for pure NbN, NbN-CoPt/MgO and CoPt-NbN/MgO bilayer systems. χ' and χ'' for all the three systems as a function of temperature have been plotted in panel (b).

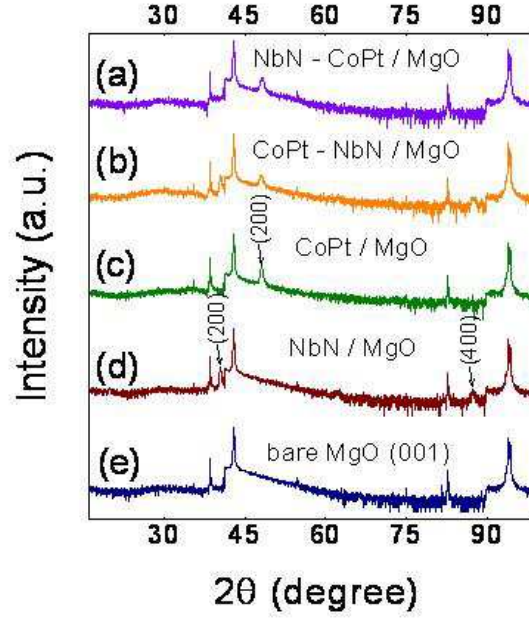


FIG. 2: (a) X-ray diffraction profiles collected with a Seifert (model 3000P) diffractometer of (a) NbN-CoPt/MgO, (b) CoPt-NbN/MgO, (c) CoPt, (d) NbN thin films deposited at 600 °C on single crystal (001) cut MgO. The diffraction profile of single crystal MgO (001) is also shown at the bottom panel. In panel (c) and (d) peaks of A1 phase CoPt and rocksalt NbN respectively are identified with miller indices.

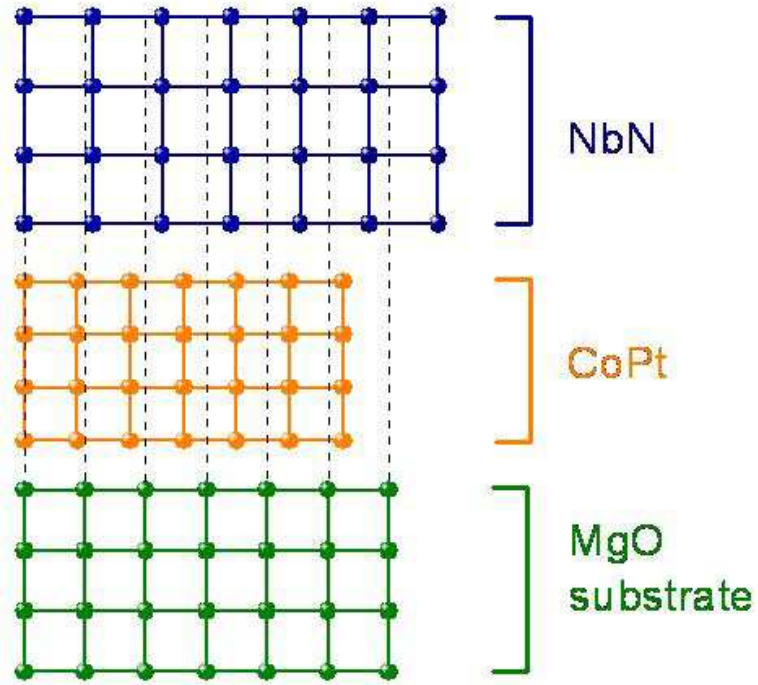


FIG. 3: Schematic illustration of strained NbN-CoPt/MgO heterostructure. Dotted lines in the figure represents ideal coherent epitaxy. Lattice mismatch is exaggerated for clarity.

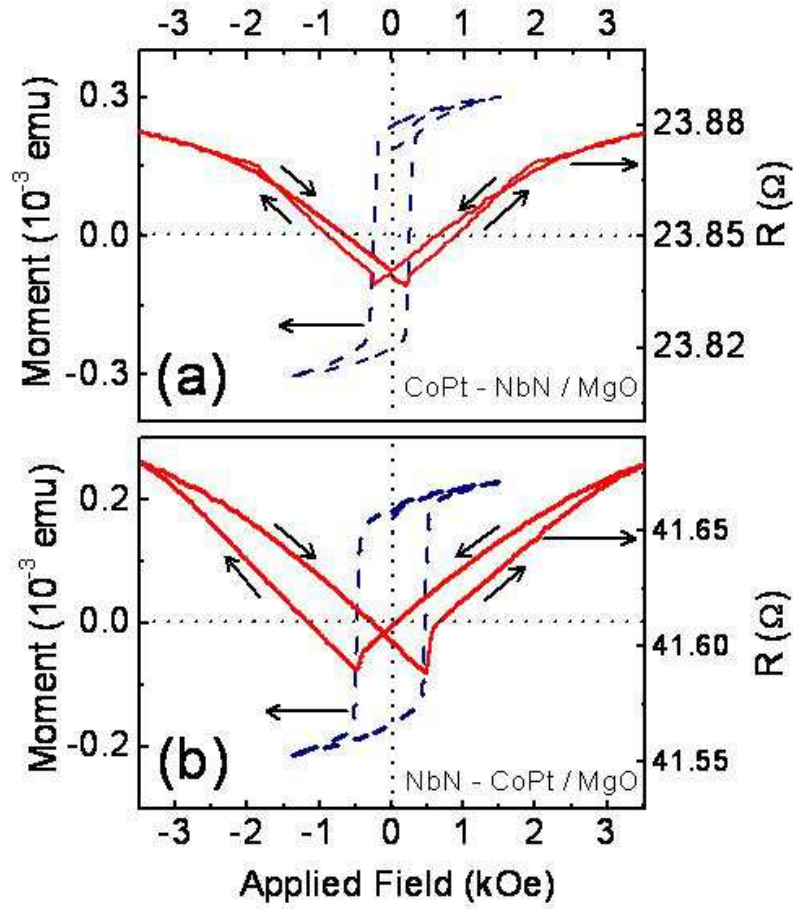


FIG. 4: Panel (a) shows isothermal magnetization and resistance as a function of magnetic field applied in-plane for CoPt-NbN/MgO system measured at 20 K. Panel (b) shows the dependence of magnetization and resistance on in-plane magnetic field for NbN-CoPt/MgO system measured at 20 K. Arrows in the figure mark the behavior of resistance on increasing and decreasing field sweeps.

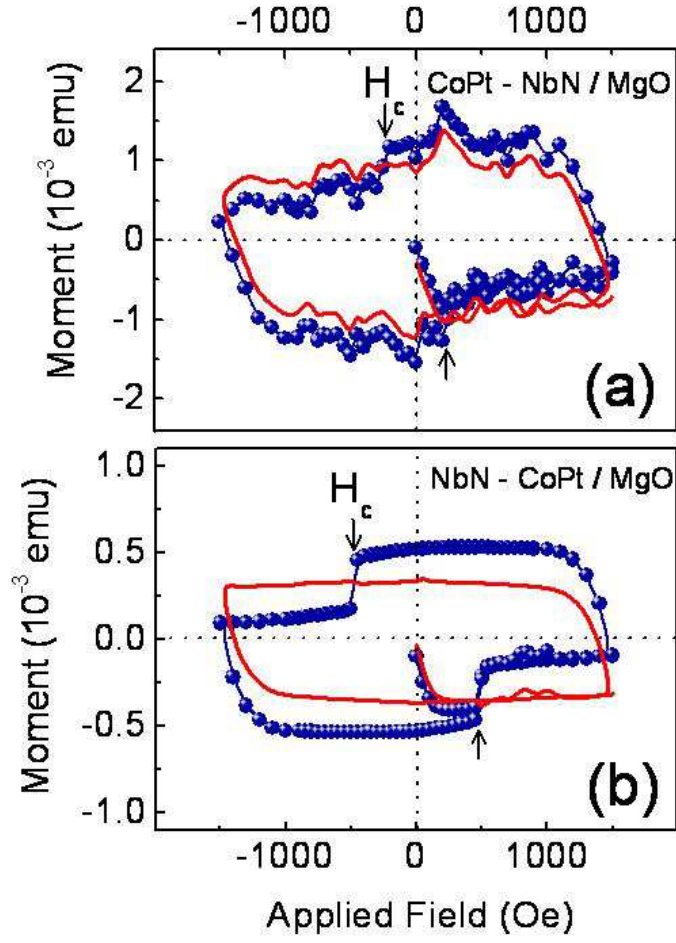


FIG. 5: Panels (a) and (b) show the in-plane magnetization as a function of applied magnetic field measured at 5 K for CoPt-NbN/MgO and NbN-CoPt/MgO system respectively. Contribution of superconducting NbN to total magnetization is extracted by subtracting 5 K data from 20 K data and is shown in the figures as continuous line.

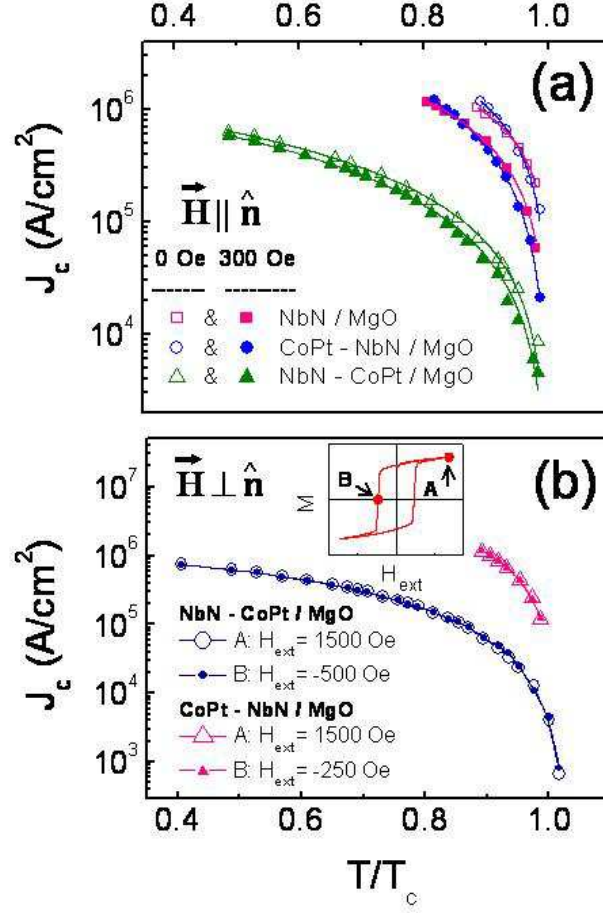


FIG. 6: (a) Plot of critical current density J_c calculated from current-voltage characteristics using a field criterion of $10 \mu\text{V}/\text{cm}$ of NbN, CoPt-NbN/MgO and NbN-CoPt/MgO as a function of reduced temperature. Open symbols and solid symbols represent the data for zero-field and 300 Oe perpendicular field ($\vec{H} \parallel \hat{n}$) measurements respectively, where \hat{n} is unit vector normal to the plane of the film. (b) Temperature dependence of J_c with in-plane magnetic field for both the bilayers. In the inset letters A and B mark the points on a typical M-H loop at which the measurements of J_c were carried out. While open symbols in panel (b) represent data taken at point A, J_c values for fully demagnetized state (point B) are plotted as solid symbols.

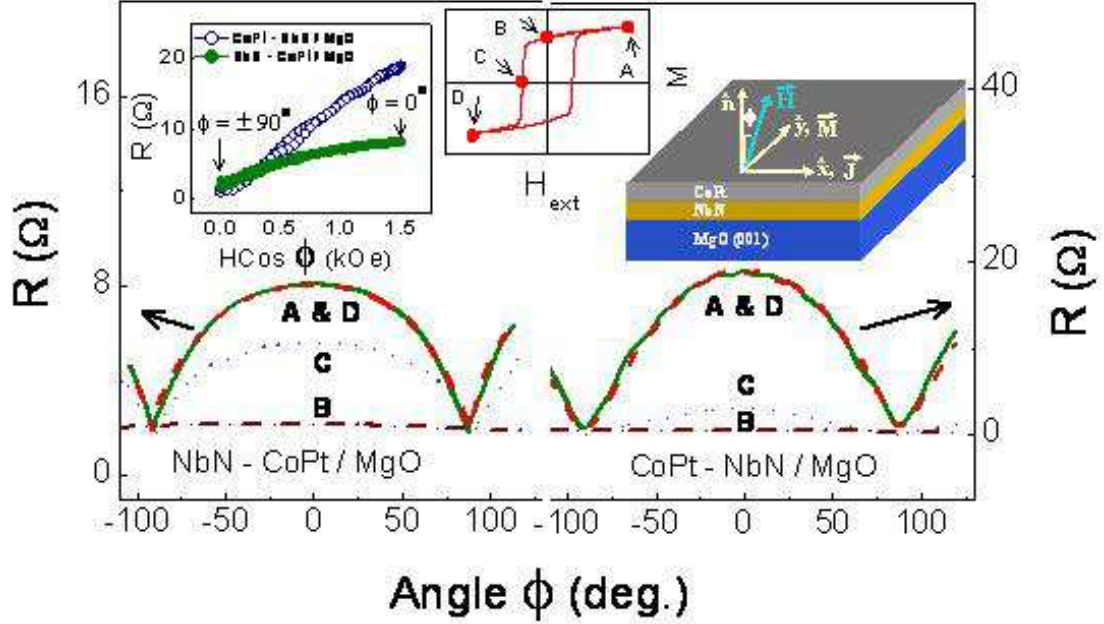


FIG. 7: The resistance of both CoPt-NbN/MgO (right Y-axis) and NbN-CoPt/MgO (left Y-axis) systems in the flux flow regime as a function of the angle ϕ between the applied magnetic field and film normal (\hat{n}) at a temperature in the transition region, where the sample resistance is 5 % of the zero-field normal state resistance. Magnetic field direction was changed in a step of 2 degree while it remained always orthogonal to the current direction ($\vec{H} \perp \vec{J}$). Zeroes on the X-axis correspond to field angle normal to the film surface. A constant bias current of 1 μ A was used for all the measurements. Right inset shows schematically the direction of current flow (\vec{J}), magnetization vector (\vec{M}) and the direction of magnetic field (\vec{H}) which makes angle ϕ with \hat{n} . The letters A, B, C and D in the middle panel mark the points on a typical M-H loop at which R was measured. Left inset shows the dependence of resistance extracted from the data presented in the main panel (curves A and D) as a function of normal component of the applied field for both the samples.

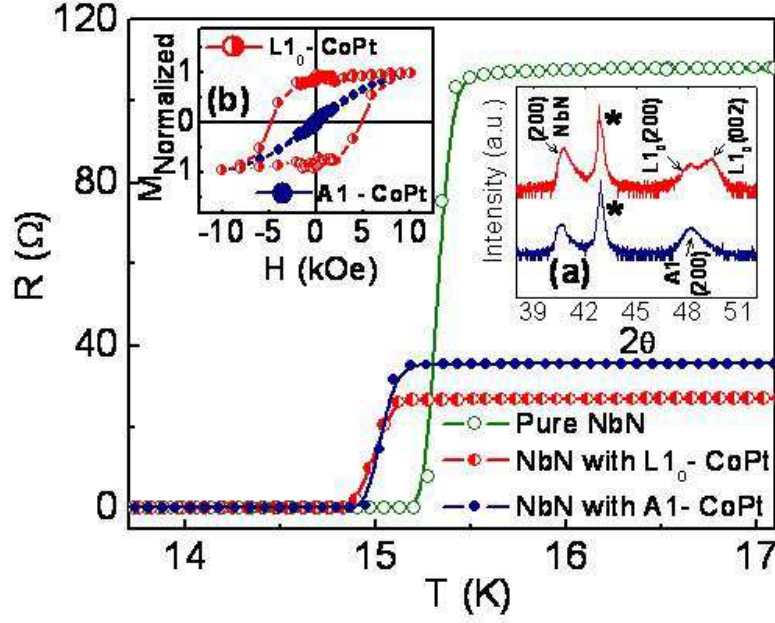


FIG. 8: Temperature dependence of resistance of CoPt-NbN/MgO bilayers with both A1 and $L1_0$ phase CoPt is compared with that of pure NbN film. Unlike the $R(T)$ plot presented in Fig. 1(a), here the NbN layer was deposited at 700 °C for all the three systems. X-ray diffraction profiles collected with X'Pert PRO MPD diffractometer of the same set of bilayer samples are shown in the inset (a). Peaks of rocksalt NbN, and A1 and $L1_0$ phase CoPt are identified with miller indices. The diffraction peak arises from the substrate is marked with asterisk. Inset (b) shows the isothermal magnetization with perpendicular magnetic field measured at 20 K for both the bilayers.

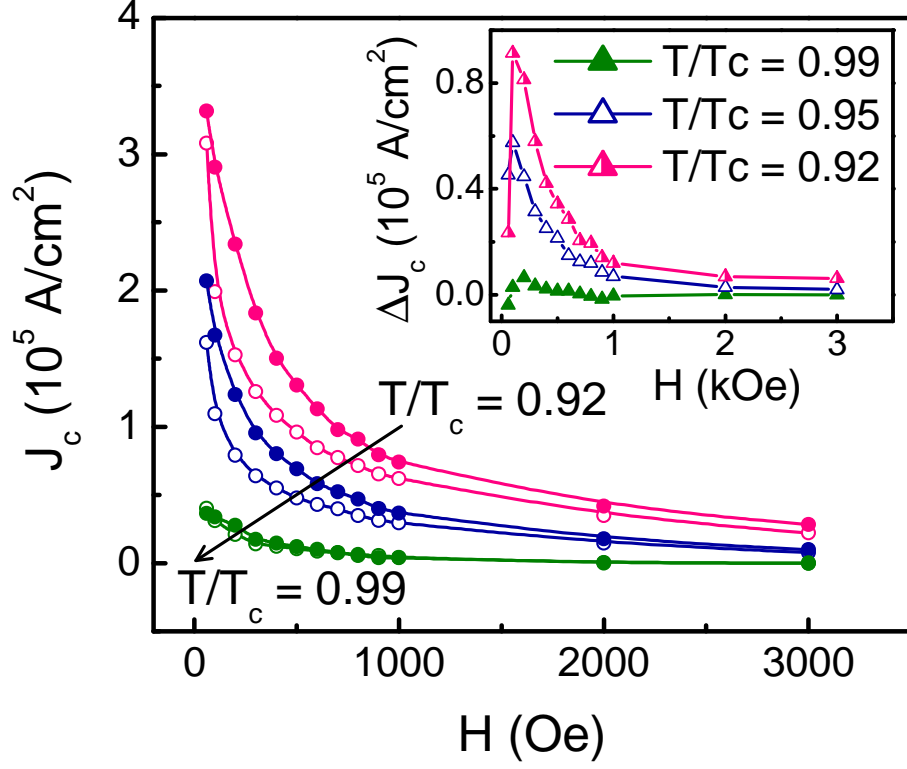


FIG. 9: Plot of critical current density J_c of (L1₀)-CoPt-NbN/MgO (solid symbols) and (A1)-CoPt-NbN/MgO (open symbols) at three different temperatures ($T/T_c = 0.99$, 0.95 and 0.92) as a function of magnetic field. The magnetic field was directed perpendicular to the plane of the film. The first data point corresponds to 60 Oe remanent field of the electromagnet. Inset shows the plot of $\Delta J_c [= J_c(\text{L1}_0) - J_c(\text{A1})]$ derived from the data shown in the main panel.